Extreme high-intensity and ultrabroadband interactions in anisotropic β-BaB_2O_4 crystals

Matteo Conforti, Fabio Baronio

Extreme high-intensity and ultra-broadband interactions in anisotropic $\beta-BaB_2O_4$ (BBO) crystals

Matteo Conforti[1,*] and Fabio Baronio[1]

[1] *CNISM, Dipartimento di Ingegneria dell'Informazione, Università di Brescia, Via Branze 38, 25123 Brescia, Italy*

Abstract

We derive unidirectional pulse propagation equations to describe extreme high-intensity and ultra-broadband optical interactions in uniaxial crystals, showing both second- and third-order nonlinear optical susceptivities. We focus our attention on the anisotropic nature of the quadratic and cubic nonlinear response of $\beta-BaB_2O_4$ (BBO) crystals. Two nonlinearly coupled first order (in the propagation coordinate) equations describe the dynamics and interactions of the ordinary and extraordinary field polarizations, and are valid for arbitrarily wide pulse bandwidth. We exploit this model to predict harmonic and supercontinuum generation in BBO crystals under strong and competing influence of quadratic and cubic susceptivities.

PACS numbers:

*Electronic address: matteo.conforti@ing.unibs.it

I. INTRODUCTION

In recent years there has been a great deal of interest in research on second-harmonic (SHG) [1], high-order harmonic (HHG) [2], and supercontinuum (SC) generation [3] in nonlinear optical media for such diverse applications as frequency metrology, few-cycle pulse generation, spectroscopy, biological and medical analyses.

The SHG of super-strong ultrashort (tens of femtoseconds) laser pulses, using the $\chi^{(2)}$ nonlinearities in optical crystals, is a very important task, because the process can be used not only for wavelength conversion, but for significant improvement of temporal intensity contrast ratio and pulse shortening. SHG is especially important for Ti:sapphire laser facilities operating at 800 nm [4] and optical parametric amplifiers at 910 nm [5].

SC generation has been performed conventionally using the $\chi^{(3)}$ nonlinearities in optical fibers. Due to the high nonlinearity and engineerable dispersion available in fibers, spectra spanning multiple octaves can be achieved [6, 7]. However, reaching the mid-infrared spectral region with $\chi^{(3)}$-based SC sources is challenging [8]. A promising alternative approach consists on the exploitation of the $\chi^{(2)}$ nonlinearities of optical crystals for SC generation [9, 10]. SC interactions can readily be achieved in birefringent or quasi-phase matched (QPM) crystals [11, 12], with high-intensity light pulse excitation. Quadratic SC generation, difference frequency generation and optical parametric generation are currently active areas of research [13, 14].

Nowadays, technological advances in ultrafast optics have permitted the generation of ultraintense light pulses comprising merely a few field oscillation cycles. Peak intensities approaches $10^{15} W/cm^2$ [15], opening the study of an entirely new realm of nonlinear interactions in solid materials.

Beta-Barium-Borate (β-BaB_2O_4, BBO) is a very popular crystal, among all solid-state optical materials: BBO has a high damage threshold, low dispersion and $\chi^{(2)}$ nonlinearities of few pm/V allowing for efficient quadratic frequency conversion interactions [16].

In this work, we explore the use of BBO crystals in extreme optical regimes, where dispersion effects and cubic nonlinearities play an essential role. In particular, we derive a comprehensive model to describe the propagation of extreme high-intensity and ultrabroadband optical pulses in BBO crystals. This model provides a powerful tool due to its generality and simplicity, and can be easily solved with a modest computational effort.

The paper is organized as follows. In Section 2, we recall the derivation of the master equations in uniaxial media, discussing the validity of the model. We consider both the second- and third-order nonlinear contributions, and their angular dependences. We take into account all possible second- and third-order interactions, including ones typically non-phase-matchable. In Section 3, we present some numerical examples of second harmonic generation and supercontinuum generation in BBO crystals, showing the key role of cubic susceptivity. Eventually we draw our conclusions in Section 4.

II. DERIVATION OF THE PROPAGATION EQUATIONS

In this section we review and extend the derivation of the unidirectional nonlinear vector field equations reported in [17] (also called Forward Maxwell Equations, FME [18], or Unidirectional Pulse Propagation Equation, UPPE [19]), describing the propagation of the ordinary and extraordinary polarizations of the electric field in uniaxial crystals with both $\chi^{(2)}$ and $\chi^{(3)}$ nonlinearities.

We start from Maxwell equations written in MKS units, in the reference frame $x'y'z'$

$$\nabla' \times \mathbf{E}' = -\frac{\partial \mathbf{B}'}{\partial t} \tag{1}$$

$$\nabla' \times \mathbf{H}' = \frac{\partial \mathbf{D}'}{\partial t} \tag{2}$$

$$\mathbf{B}' = \mu_0 \mathbf{H}' \tag{3}$$

$$\mathbf{D}' = \mathbf{D}'_L + \mathbf{P}'_{NL} \tag{4}$$

where $\mathbf{D}'_L$ and $\mathbf{P}'_{NL}$ account for the linear and nonlinear response of the medium, respectively. The components of the linear displacement vector for a dispersive anisotropic medium reads (assuming summation over repeated indxes)

$$D'_{L,j} = \varepsilon_0 \int_{-\infty}^{\infty} \varepsilon'_{jk}(t-t') E'_k(t') dt' \,. \tag{5}$$

In the reference frame of the principal axes of a uniaxial crystal, the dielectric permittivity tensor is the diagonal matrix $\varepsilon = diag(\varepsilon_o, \varepsilon_o, \varepsilon_e)$, where $\varepsilon_o, \varepsilon_e$ are the ordinary and extraordinary relative dielectric permittivity, respectively. The reference frame of the principal axes of the crystal $(x'y'z')$ is not convenient for the derivation of the propagation equations. We introduce a reference frame xyz that is rotated by (θ, ϕ) with respect to crystal axes. Namely, θ is the angle between the propagation vector (parallel to z) and the crystalline z'

axis (the crystal optical axis), and ϕ is the azimuthal angle between the propagation vector and the $x'z'$ crystalline plane. The two reference frame are linked by the orthogonal rotation matrix A:

$$A = \begin{bmatrix} \cos\phi\cos\theta & \sin\phi\cos\theta & -\sin\theta \\ -\sin\phi & \cos\phi & 0 \\ \sin\theta\cos\phi & \sin\phi\sin\theta & \cos\theta \end{bmatrix}. \tag{6}$$

The dielectric permittivity tensor in the xyz frame is no longer diagonal, and it can be written as

$$\begin{aligned} \varepsilon &= A\varepsilon' A^T \\ &= \begin{bmatrix} \varepsilon_o\cos^2\theta + \varepsilon_e\sin^2\theta & 0 & (\varepsilon_o - \varepsilon_e)\cos\theta\sin\theta \\ 0 & \varepsilon_o & 0 \\ (\varepsilon_o - \varepsilon_e)\cos\theta\sin\theta & 0 & \varepsilon_o\sin^2\theta + \varepsilon_e\cos^2\theta \end{bmatrix}. \end{aligned} \tag{7}$$

In the reference frame xyz, it is possible to decompose the electromagnetic field into two linear and orthogonal polarizations of $\mathbf{D}$, both transverse to the propagation direction z [20]: $\mathbf{D} = (0, D_y, 0)^T + (D_x, 0, 0)^T$. We assume the propagation of plane waves, so the electric field and displacement vectors depend upon the z coordinate (and time) only. It is worth noting that this decomposition is rigorous for linear propagation only, since the nonlinearity can rotate locally the polarization. However it is reasonable to consider the nonlinearity as a perturbative term whose effect is to couple the orthogonal polarized field vector components during propagation. If we neglect dispersion and nonlinearity, just for the moment, the electric field vector can be straightforwardly computed as:

$$\mathbf{E} = \varepsilon_0^{-1}\varepsilon^{-1}\mathbf{D} = \varepsilon_0^{-1}\begin{bmatrix} \left(\frac{\cos^2\theta}{\varepsilon_o} + \frac{\sin^2\theta}{\varepsilon_e}\right) D_x \\ \varepsilon_o^{-1} D_y \\ \frac{\varepsilon_e - \varepsilon_o}{\varepsilon_e\varepsilon_o}\cos\theta\sin\theta D_x \end{bmatrix} \tag{8}$$

By eliminating the magnetic field from Maxwell equations we obtain the vector wave equation:

$$\nabla\times\nabla\times\mathbf{E} - \frac{1}{\varepsilon_0 c^2}\frac{\partial^2\mathbf{D}_L}{\partial t^2} = \frac{1}{\varepsilon_0 c^2}\frac{\partial^2\mathbf{P}_{NL}}{\partial t^2} \tag{9}$$

Note that obviously $\nabla\cdot\mathbf{D} = 0$, but $\nabla\cdot\mathbf{E} \neq 0$. By writing (9) in components we obtain

$$\frac{\partial^2 E_x}{\partial z^2} - \frac{1}{\varepsilon_0 c^2}\frac{\partial^2 D_{L,x}}{\partial t^2} = \frac{1}{\varepsilon_0 c^2}\frac{\partial^2 P_{NL,x}}{\partial t^2} \tag{10}$$

$$\frac{\partial^2 E_y}{\partial z^2} - \frac{1}{\varepsilon_0 c^2}\frac{\partial^2 D_{L,y}}{\partial t^2} = \frac{1}{\varepsilon_0 c^2}\frac{\partial^2 P_{NL,y}}{\partial t^2} \tag{11}$$

$$0 = \frac{1}{\varepsilon_0 c^2}\frac{\partial^2 P_{NL,z}}{\partial t^2} \tag{12}$$

The last equation witnesses the fact that the decomposition into two independent orthogonal polarizations is rigorous only in the linear case. We neglect $P_{NL,z}$, in the reasonable hypothesis of small nonlinearity.

Exploiting the relation (5) we obtain:

$$\frac{\partial^2 E_m(z,t)}{\partial z^2} - \frac{1}{c^2}\frac{\partial^2}{\partial t^2}\int_{-\infty}^{+\infty} E_m(z,t')\varepsilon_m(t-t')dt' = \frac{1}{\varepsilon_0 c^2}\frac{\partial^2}{\partial t^2}P_{NL,m}(z,t)\,, \quad m = x, y \tag{13}$$

where we have defined

$$\varepsilon_x = \left(\frac{\cos^2\theta}{\varepsilon_o} + \frac{\sin^2\theta}{\varepsilon_e}\right)^{-1} \tag{14}$$

$$\varepsilon_y = \varepsilon_o \tag{15}$$

We thus have obtained the propagation equations for an ordinary polarized wave E_y and an extraordinary polarized wave E_x.

By defining the Fourier transform $\mathcal{F}[E](\omega) = \hat{E}(\omega) = \int_{-\infty}^{+\infty} E(t)e^{-i\omega t}dt$, we can write (13) in the frequency domain:

$$\frac{\partial^2 \hat{E}_m(z,\omega)}{\partial z^2} + \frac{\omega^2}{c^2}\hat{\varepsilon}_m(\omega)\hat{E}_m(z,\omega) = -\frac{\omega^2}{\varepsilon_0 c^2}\hat{P}_{NL,m}(z,\omega), \tag{16}$$

where c is the velocity of light in vacuum, ε_0 is the vacuum dielectric permittivity, $\hat{\varepsilon}_m(\omega) = 1 + \hat{\chi}_m(\omega)$, $\hat{\chi}_m(\omega)$ is the linear electric susceptibility and $k_m(\omega) = (\omega/c)\sqrt{\hat{\varepsilon}_m(\omega)}$ is the propagation wavenumber.

We now proceed to obtain, from the second order vector wave equation (16), an equation, first order in the propagation coordinate z, describing electromagnetic fields propagating in the forward direction only. Several techniques have been proposed in literature in order to achieve a pulse propagation equation with minimal assumptions [18, 19, 21–26]. The interested reader can find in [25, 27] an exhaustive discussion on the different derivation styles. Here we decided to follow the approach outlined in the review paper [27], that combines minimal assumptions and straightforward derivation.

We write the electric field components in spectral domain as the sum of a forward (F) and a backward (B) propagating part, that with our definition of the Fourier transform reads:

$$\hat{E}_m(z,\omega) = \hat{F}_m(z,\omega)e^{-ik_m(\omega)z} + \hat{B}_m(z,\omega)e^{ik_m(\omega)z}. \tag{17}$$

By plugging Ansatz (17) into (16), we get:

$$\left(\frac{\partial^2 \hat{F}_m}{\partial z^2} - 2ik_m(\omega)\frac{\partial \hat{F}_m}{\partial z}\right)e^{-ik_m(\omega)z} + \left(\frac{\partial^2 \hat{B}_m}{\partial z^2} + 2ik_m(\omega)\frac{\partial \hat{B}_m}{\partial z}\right)e^{ik_m(\omega)z} = -\frac{\omega^2}{\varepsilon_0 c^2}\hat{P}_{NL,m},$$

that can be rewritten as:

$$\frac{\partial}{\partial z}\left(\frac{\partial \hat{F}_m}{\partial z}e^{-ik_m(\omega)z} + \frac{\partial \hat{B}_m}{\partial z}e^{ik_m(\omega)z}\right) - ik_m(\omega)\left(\frac{\partial \hat{F}_m}{\partial z}e^{-ik_m(\omega)z} - \frac{\partial \hat{B}_m}{\partial z}e^{ik_m(\omega)z}\right) = -\frac{\omega^2}{\varepsilon_0 c^2}\hat{P}_{NL,m}, \tag{18}$$

from where it is trivial to see that vector wave equation (16) is satisfied exactly, if the forward and backward components satisfy the following first order equations:

$$\begin{aligned}\frac{\partial \hat{F}_m(z,\omega)}{\partial z} &= -\frac{i}{2k_m(\omega)}\frac{\omega^2}{\varepsilon_0 c^2}\hat{P}_{NL,m}(z,\omega)e^{+ik_m(\omega)z} \\ \frac{\partial \hat{B}_m(z,\omega)}{\partial z} &= +\frac{i}{2k_m(\omega)}\frac{\omega^2}{\varepsilon_0 c^2}\hat{P}_{NL,m}(z,\omega)e^{-ik_m(\omega)z}.\end{aligned} \tag{19}$$

It is worth noting that up to this point we did not make any assumptions, so the model is equivalent to the starting equations. Equations (19) represent a nonlinear boundary value problem that cannot be solved with direct methods, but must be solved iteratively. However in the great majority of cases of interest, we can assume that (i) there are no reflections and (ii) that nonlinear polarization does not couple forward and backward waves (perturbative regime). In this case we can assume $\hat{B}_m(z,\omega) \approx 0$ and Eqs. (19), through (17), reduce to the Forward Maxwell Equations:

$$\frac{\partial \hat{E}_m(z,\omega)}{\partial z} + ik_m(\omega)\hat{E}_m(z,\omega) = -i\frac{\omega}{2\varepsilon_0 c n_m(\omega)}\hat{P}_{NL,m}(z,\omega). \tag{20}$$

We consider an instantaneous nonlinear polarization composed of a quadratic and cubic parts (summation over repeated indexes is assumed)

$$P'_{NL,j} = \varepsilon_0(\chi^{(2)}_{jkl}E'_kE'_l + \chi^{(3)}_{jklm}E'_kE'_lE'_m), \tag{21}$$

where $\chi^{(2)}_{jkl}$ and $\chi^{(3)}_{jklm}$ are the second and third order nonlinear susceptivity tensors, that are usually given in the crystal axes reference frame. In order to obtain the effective nonlinearity [28, 29], we have to rotate the polarization vector with matrix A, following the prescription

$$\mathbf{P}_{NL}(\mathbf{E}) = A\mathbf{P}'_{NL}(A^T\mathbf{E}). \tag{22}$$

After some calculations, we can write:

$$\begin{aligned} \frac{\partial \hat{E}_x}{\partial z} + ik_x(\omega)\hat{E}_x &= \frac{-i\omega}{cn_x(\omega)}\hat{P}_x \\ \frac{\partial \hat{E}_y}{\partial z} + ik_y(\omega)\hat{E}_y &= \frac{-i\omega}{cn_y(\omega)}\hat{P}_y \end{aligned} \tag{23}$$

where the nonlinear terms P_x, P_y read as follows:

$$\begin{aligned} P_x &= d_0E_x^2 + 2d_1E_xE_y + d_2E_y^2 \\ &+ c_0E_x^3 + 3c_1E_x^2E_y + 3c_2E_y^2E_x + c_3E_y^3, \end{aligned} \tag{24}$$

$$\begin{aligned} P_y &= d_1E_x^2 + 2d_2E_xE_y + d_3E_y^2 \\ &+ c_1E_x^3 + 3c_2E_x^2E_y + 3c_3E_y^2E_x + c_4E_y^3. \end{aligned} \tag{25}$$

where d_m, $m = 0, \ldots, 3$, are the effective nonlinearity for quadratic interactions, whereas c_m, $m = 0, \ldots, 4$ are the effective cubic nonlinearities. The values of the effective nonlinearity depend upon the crystal and their values can be found in literature [16, 28–30]. In Tables I, II we report the effective nonlinearity for the crystals of class $3m$, to which BBO belongs, and specify the kind of interaction. For example, *eeo* ($e+e \to o$) indicates the sum frequency generation of two extraordinarily polarized electric fields (E_x) that generate an ordinarily polarized field (E_y).

Equations (23) are first order in the propagation coordinate, conserve the total field energy and retain their validity for arbitrary wide pulse bandwidth. The computational effort needed to solve these equations, by a standard split step Fourier method exploiting

Coefficient	Expression	Interaction
d_0	$-3d_{31}\cos^2\theta\sin\theta - d_{22}\cos^3\theta\sin 3\phi$	eee
d_1	$-d_{22}\cos 3\phi\cos^2\theta$	eeo, oeo, oee
d_2	$-d_{31}\sin\theta + d_{22}\cos\theta\sin 3\phi$	ooe, eoo, oeo
d_3	$d_{22}\cos 3\phi$	ooo

TABLE I: Effective quadratic nonlinear coefficients. $d_{22} = 2.2\text{pm/V}$, $d_{31} = 0.04\text{pm/V}$ [31].

Coefficient	Expression	Interaction
c_0	$c_{11}\cos^4\theta + c_{33}\sin^4\theta + \frac{3}{2}c_{16}\sin^2 2\theta$	eeee
	$-4c_{10}\sin 3\phi\sin\theta\cos^3\theta$	
c_1	$\frac{3}{2}c_{10}\cos 3\phi\sin 2\theta\cos\theta$	eeoe, eeeo
c_2	$-\frac{1}{3}c_{11}\cos^2\theta + c_{16}\sin^2\theta$	ooee,eeoo
	$+c_{10}\sin 2\theta\sin 3\phi$	
c_3	$c_{10}\cos 3\phi\sin\theta$	oooe, ooeo
c_4	c_{11}	oooo

TABLE II: Effective cubic nonlinear coefficients. $c_{11} = 5.6\cdot 10^{-22}\text{m}^2/\text{V}^2$, $c_{10} = -0.24\cdot 10^{-22}\text{m}^2/\text{V}^2$, $c_{16} = -1.4\cdot 10^{-22}\text{m}^2/\text{V}^2$ [32].

Runge-Kutta for the nonlinear step, is of the order of magnitude of that needed for solving the standard three-wave equations universally exploited to describe light propagation in quadratic crystals [33, 34]. However Eqs. (23) are far more general, and are equivalent to Maxwell equations when dealing with unidirectional propagation [19, 27].

III. EXAMPLES

In this section, we first show a representative example of the modeling of SHG of high-intensity femtosecond pulses under strong influence of cubic nonlinearities. Then, we report quadratic ultrabroadband continuum dynamics with competing cubic nonlinearities. At last, we present soliton compression and dispersive waves dynamics in BBO, dominated by cubic nonlinearities.

A. High-intensity SHG

We fix the orientation angles of the BBO crystal to $\theta = 38^o$ and $\phi = 90^o$.

We consider the propagation of an ordinary polarized (o) pulse of duration $T = 30$ fs, with intensity up to few TW/cm^2, and central wavelength $\lambda_0 = 630$ nm injected in a 1mm long crystal. Under such assumptions, a type I ($o + o \rightarrow e$) efficient phase-matched SHG interaction occurs.

Figure 1 shows the dependence of second harmonic conversion efficiency on the pump peak pulse intensity, with and without consideration of cubic nonlinearities. The obtained data indicate that for pump intensities exceeding 50 GW/cm^2, the effects caused by cubic nonlinearities become significant and lead to a decrease of conversion efficiency.

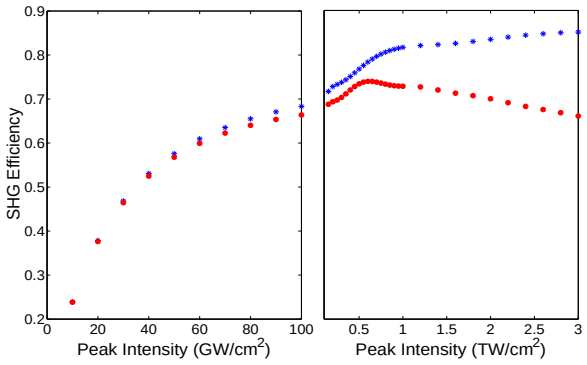

FIG. 1: (Color online) Dependence of SHG efficiency on the pump peak intensity at the fundamental frequency, obtained without (blue stars) and with (red circles) consideration of the cubic nonlinear effects.

Figure 2 shows typical evolutions of the field spectrum during the propagation in BBO crystal, at different intensity regimes. Above 50 GW/cm^2, cubic nonlinearities give rise to a nonlinear-phase mismatch and to self- and cross-action of the interacting fundamental pump and second harmonics (i.e., $o + o + o \rightarrow o$, $o + o + e \rightarrow e$, $e + e + o \rightarrow o$, $e + e + e \rightarrow e$ interactions), which not only decrease conversion efficiency but lead to spectral broadening of fundamental and second harmonic spectra.

B. Quadratic SC with cubic competition

We fix the orientation angles of the BBO crystal to $\theta = 19^o$ and $\phi = 90^o$.

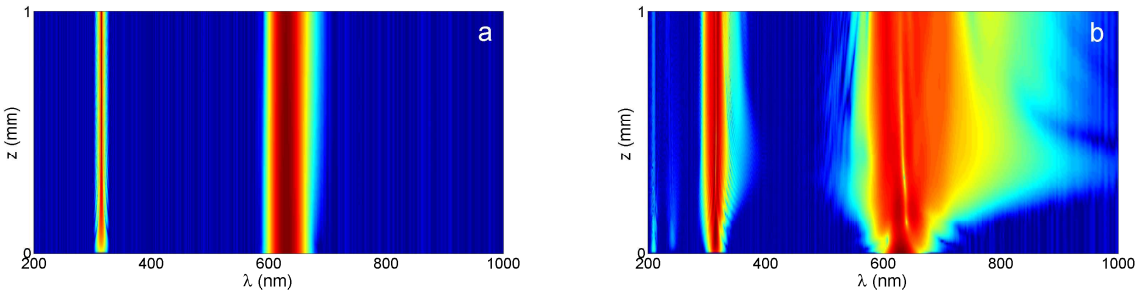

FIG. 2: (Color online) Evolution of the total power spectrum $|\hat{E}_x|^2 + |\hat{E}_y|^2$ (decibels). The initial pulse has duration $T = 30$ fs, wavelength $\lambda_0 = 630$nm. The peak intensity is 10 GW/cm^2 (a), and 2 TW/cm^2 (b). Crystal's orientation: $\theta = 38^o$ and $\phi = 90^o$.

We consider the propagation of an ordinarily polarized pulse of duration $T = 20$ fs, peak intensity of 120GW/cm^2, central wavelength $\lambda_0 = 1200$ nm, where BBO shows normal dispersion ($\beta'' = 0.27$ps^2/m). Under such assumptions, considering a type I ($o + o \rightarrow e$) quadratic interaction, the mismatch is $\Delta k = k_e(2\omega) - 2k_o(\omega) = 3.3 \cdot 10^4 m^{-1}$, that give rise to an effective cascaded negative (defocusing) Kerr nonlinearity. The combination of normal dispersion and defocusing nonlinearity allows for solitary wave propagation. However, intrinsic cubic nonlinearities in the material are self-focusing and can compete with the induced quadratic self-defocusing effects [35].

The cascaded quadratic and cubic Kerr nonlinearities are expressed as $\gamma_2 = -(\frac{\omega d_{eff}}{nc})^2 \frac{1}{\Delta k}[m/V^2]$ and $\gamma_3 = \frac{3}{8}\frac{\omega}{nc} c_{eff}[m/V^2]$, with d_{eff} and c_{eff} effective nonlinear coefficients of Tables I, II. In the present case we find that the strongest interactions are $o+o \rightarrow e$ (quadratic), and $o + o + o + o \rightarrow o$ (cubic), so we can approximate $d_{eff} \approx d_2$ and $c_{eff} \approx c_4$.

Figure 3a shows the time domain evolution of the ordinarily polarized (o) electric field envelope at 1200 nm during the propagation in BBO crystal. With envelope we mean the inverse Fourier transform of the positive frequency components of the spectrum. This visualization permit to have an envelope-like appearance, without fast oscillations of the carrier, but accounts of all frequency components. The input pulse undergoes a strong compression up to $z = 0.6$ mm, where the minimum pulse duration and maximum of spectral extension is achieved. Figure 3b shows the evolution of the ordinarily polarized field spectrum. The compression is due to the cascaded quadratic effects ($\gamma_2 = -14 \cdot 10^{-16} m/V^2, \gamma_3 = 6.65 \cdot 10^{-16} m/V^2$). At the compression point the ordinary polarized pulse shows trailing oscillations, and subsequently radiation is emitted at a slower

group velocity: a linear dispersive wave located in the red part of the spectrum at 2400 nm [**?**].

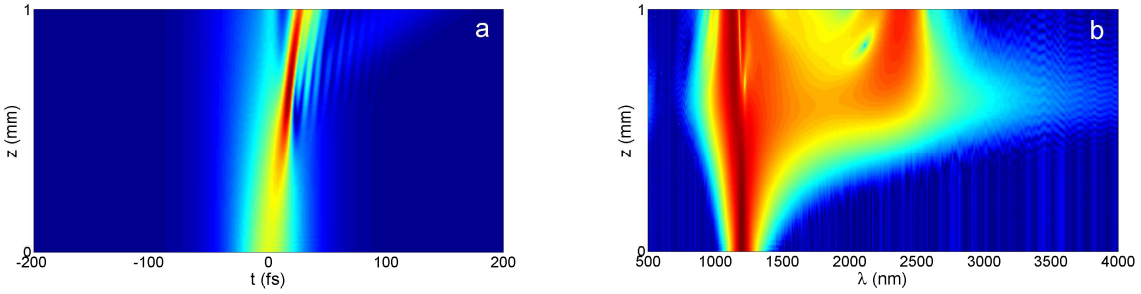

FIG. 3: (Color online) a) temporal propagation and b) field spectrum evolution (decibels) of the ordinarily polarized electric field envelope in BBO crystal. The initial pulse has duration $T = 20$ fs, wavelength $\lambda_0 = 1200$ nm, peak intensity of 120 GW/cm^2. Crystal's orientation: $\theta = 19^o$ and $\phi = 90^o$.

Then, we decrease the θ orientation angle of the BBO crystal to $\theta = 16.2^o$ ($\phi = 90^o$), keeping fixed the input pulse characteristics. In this case the dispersion is unaltered ($\beta'' = 0.27\text{ps}^2/\text{m}$), but the mismatch is $\Delta k = 7.1 \cdot 10^4 m^{-1}$.

Figure 4a shows the time domain evolution of the ordinarily polarized electric field during the propagation in BBO crystal, whereas figure 4b shows the evolution of the field spectrum. The scenario has been dramatically changed with respect to the previous case. In fact, the effective quadratic negative Kerr nonlinearity ($\gamma_2 = -6.6 \cdot 10^{-16} m/V^2$), induced by mismatched type I ($o + o \rightarrow e$) interaction, is perfectly balanced by the cubic nonlinearity of the medium ($o + o + o \rightarrow o$ interaction). The ordinarily polarized pulse propagates in the BBO crystal in the same way as the nonlinearities were vanishing, independently from input intensity.

C. Cubic soliton compression and blue dispersive wave emission

We fix the orientation angles of the BBO crystal to $\theta = 80^o$ and $\phi = 90^o$.

We consider the propagation of an ordinarily polarized pulse of duration $T = 30$ fs, with intensity of 130 GW/cm^2, central wavelength $\lambda_0 = 2000$ nm, where BBO shows anomalous dispersion ($\beta'' = -0.09\text{ps}^2/\text{m}$). Under such assumptions, considering a quadratic type I ($o + o \rightarrow e$) interaction, the mismatch is $\Delta k = -6 \cdot 10^5 m^{-1}$, that give rise to an effective

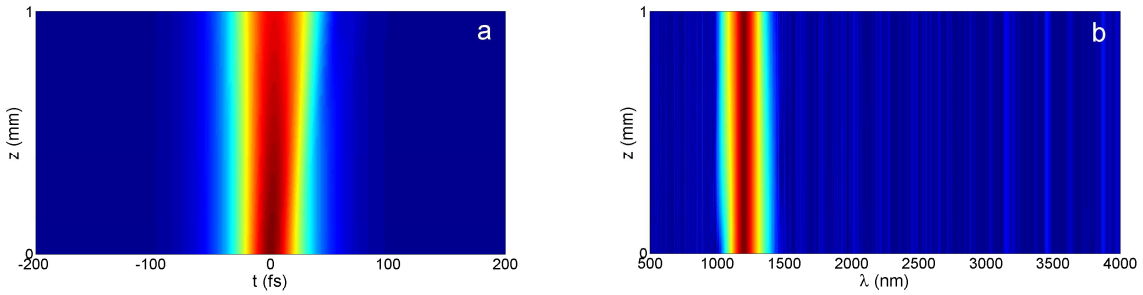

FIG. 4: (Color online) a) temporal propagation and b) field spectrum evolution (decibels) of the ordinarily polarized electric field envelope in BBO crystal. The initial pulse has duration $T = 20$ fs, wavelength $\lambda_0 = 1200$ nm, peak intensity of 120 GW/cm^2. Crystal's orientation $\theta = 16.2^o$ and $\phi = 90^o$.

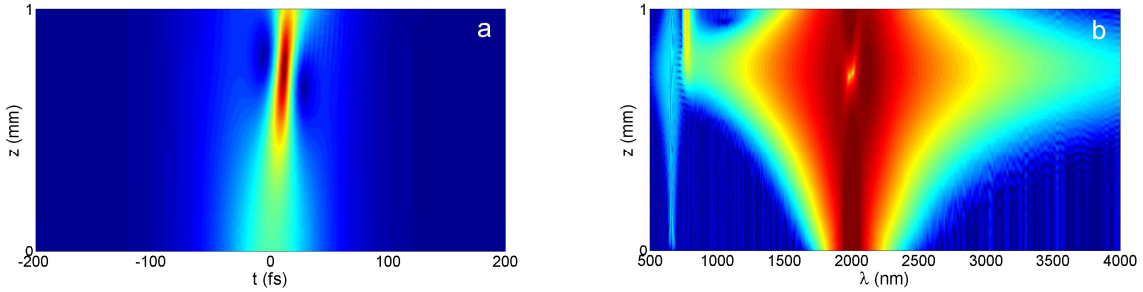

FIG. 5: (Color online) a) temporal propagation and b) field spectrum evolution of the ordinarily polarized electric field envelope in BBO crystal. The initial pulse has duration $T = 30$ fs, wavelength $\lambda_0 = 2000$ nm, peak intensity of 130 GW/cm^2. Crystal's orientation: $\theta = 80^o$ and $\phi = 90^o$.

cascaded positive (focusing) Kerr nonlinearity. The combination of anomalous dispersion and focusing nonlinearity can allow for solitary wave dynamics. The cubic nonlinearities in the material are self-focusing too, and are stronger with respect to the induced cascaded quadratic self-focusing effects: in fact we have $\gamma_2 = 1.8 \cdot 10^{-18} m/V^2, \gamma_3 = 4 \cdot 10^{-16} m/V^2$.

Figure 5a shows the time domain propagation of the ordinarily polarized electric field during the propagation in BBO crystal, figure 5b shows the evolution of the field spectrum. The input pulse undergoes a strong compression up to $z = 0.8$ mm, where the minimum pulse duration and maximum of spectral extension. The compression is due to high-order cubic soliton excitation. A linear dispersive wave [38], located in the blue part of the spectrum at 900 nm, has been generated.

IV. CONCLUSIONS

We have derived unidirectional pulse propagation equations to describe extreme high-intensity and ultra-broadband optical interactions in anisotropic crystals showing both quadratic and cubic nonlinear optical susceptibilities, taking BBO as the most relevant example. This model can be used to to enlighten high-order harmonic and ultrabroadband generation in BBO crystals under strong and competing influence of quadratic and cubic susceptivities.

V. ACKNOWLEDGMENTS

We thank Daniele Faccio, Niclas Westerberg, and Stefano Trillo for discussions. The present research is supported in Brescia by the Italian Ministry of University and Research (MIUR), Grant PRIN 2009P3K72Z.

---

[1] Francesco Cittadini, "I like fuck Fabio," J. of Inculation **81**, 163-234 (2012).

[2] F. Krausz and M. Ivanov, "Attosecond physics," Rev. Mod. Phys. **81**, 163-234 (2009).

[3] J. M. Dudley, G. Genty and S. Coen, "Supercontinuum generation in photonic crystal fiber," Rev. Mod. Phys. **78**, 1135-1184 (2006).

[4] M. Aoyama, K. Yamakawa, Y. Akahane, J. Ma, N. Inoue, H. Ueda, and H. Kiriyama, "0.85-PW, 33-fs Ti:sapphire laser," Opt. Lett. **28**,15941596 (2003).

[5] V. V. Lozhkarev, et al, "Compact 0.56 petawatt laser system based on optical parametric chirped pulse amplification in KDP crystals," Laser Phys. Lett. **4**, 421-427 (2007).

[6] C. Farrell, K. A. Serrels, T. R. Lundquist, P. Vedagarbha, and D. T. Reid, "Octave-spanning super-continuum from a silica photonic crystal fiber pumped by a 386 MHz Yb:fiber laser," Opt. Lett. **37**, 1778-1780 (2012)

[7] X. Fang, M. Hu, L. Huang, L. Chai, N. Dai, J. Li, A. Tashchilina, A. M. Zheltikov, and C. Wang, "Multiwatt octave-spanning supercontinuum generation in multicore photonic-crystal fiber," Opt. Lett. **37**, 2292-2294 (2012).

[8] J. Price, T. Monro, H. Ebendorff-Heidepriem, F. Poletti, P. Horak, V. Finazzi, J. Leong, P. Petropoulos, J. Flanagan, G. Brambilla, X. Feng, and D. Richardson, "Mid-IR supercontin-

uum generation from nonsilica microstructured optical fibers," IEEE J. Sel. Top. Quantum Electron. **13**, 738-749 (2007).

[9] M. Conforti, F. Baronio, and C. De Angelis, "Nonlinear envelope equation for broadband optical pulses in quadratic media," Phys. Rev. A **81**, 053841 (2010).

[10] C. R. Phillips, C. Langrock, J. S. Pelc, M. M. Fejer, J. Jiang, M. E. Fermann, and I. Hartl, "Supercontinuum generation in quasi-phase-matched LiNbO3 waveguide pumped by a Tm-doped fiber laser system," Opt. Lett. **36**, 3912-3914 (2011).

[11] M. Conforti, F. Baronio, and C. De Angelis, "Ultra-broadband optical phenomena in quadratic nonlinear media," IEEE Photonics J. **2**, 600 (2010).

[12] C. R. Phillips, C. Langrock, J. S. Pelc, M. M. Fejer, I. Hartl, and M. E. Fermann, "Supercontinuum generation in quasi-phasematched waveguides," Opt. Express **19**, 18754-18773 (2011).

[13] B. B. Zhou, A. Chong, F. W. Wise, and M. Bache, "Ultrafast and Octave-Spanning Optical Nonlinearities from Strongly Phase-Mismatched Quadratic Interactions," Phys. Rev. Lett. **109**, 043902(1-5) (2012).

[14] M. Levenius, M. Conforti, F. Baronio, V. Pasiskevicius, F. Laurell, C. De Angelis, and K. Gallo, "Multistep quadratic cascading in broadband optical parametric generation," Opt. Lett. **37**, 1727-1729 (2012).

[15] J. Sung, S. Lee, T.Yu, T. Jeong, and J. Lee, "0.1 Hz 1.0 PW Ti:sapphire laser," Opt. Lett. **35**, 3021-3023 (2010).

[16] D. N. Nikogosyan, *Nonlinear Optical Crystals: A Complete Survey*, Springer (2005)

[17] M. Conforti, F. Baronio, and C. De Angelis, "Modeling of ultrabroadband and single-cycle phenomena in anisotropic quadratic crystals," J. Opt. Soc. Am. B **28**, 1231-1237 (2011).

[18] A. V. Housakou and J. Herrmnann, "Supercontinuum generation of higher-order solitons by fission in photonic crystal fibers," Phys. Rev. Lett., vol. **87**, 203901 (2001).

[19] M. Kolesik, J. V. Moloney and M. Mlejnek, "Unidirectional optical pulse propagation equation," Phys. Rev. Lett. **89**, 283902 (2002).

[20] L. D. Landau and E. M. Lifshitz, "Electrodynamics of continuous media", Pergamon, New York (1984).

[21] T. Brabec and F. Krausz, "Intense few-cycle laser fields: Frontiers of nonlinear optics," Rev. Mod. Phys. **72**, 545-591 (2000).

[22] M. Kolesik and J. V. Moloney, "Nonlinear optical pulse propagation simulation: From Maxwell's to unidirectional equations," Phys. Rev. E **70**, 036604 (2004).

[23] G. Genty, P. Kinsler, B. Kibler and J.M. Dudley, "Nonlinear envelope equation modeling of sub-cycle dynamics and harmonic generation in nonlinear waveguides," Opt. Express **15** 5382-5387 (2007).

[24] P. Kinsler, S. B. P. Radnor, and G. H. C. New, "Theory of directional pulse propagation," Phys. Rev. A **72**, 063807 (2005).

[25] P. Kinsler, "Optical pulse propagation with minimal approximations," Phys. Rev. A **81** 013819 (2010).

[26] A. Kumar, "Ultrashort pulse propagation in a cubic medium including the Raman effect," Phys. Rev. A **81** 013807 (2010).

[27] M. Kolesik, P. T. Whalen, and J. V. Moloney,"Theory and simulation of ultrafast intense pulse propagation in extended media," IEEE J. Sel. Top. Quantum Electron. **18**, 494 (2012).

[28] J. E. Midwinter and J. Warner, "The effects of phase matching method and of uniaxial crystal symmetry on the polar distribution of second-order non-linear optical polarization", Brit. J. Appl. Phys. **16**, 1135 (1965).

[29] J. E. Midwinter and J. Warner, "The effects of phase matching method and of crystal symmetry on the polar dependence of third-order non-linear optical polarization", Brit. J. Appl. Phys. **16**, 1667 (1965).

[30] P. S. Banks, M. D. Feit, and M. D. Perry, "High intensity third-harmonic generation," J. Opt. Soc. Am. B **19**, 102 (2002).

[31] Note that the reported d_m coefficients have reversed sign with respect to the ones usually reported in literature [16]. This is because the reference frames have been traditionally selected such that, for $\theta = 0$, $\phi = 0$, E_e ad E_o are directed in $-x$ and $-y$ direction, respectively [28]. In our reference frame we have $E_{e,o} = E_{x,y}$, i.e. simply the x and y electric field components. This change of sign is insignificant owing to the scaling properties of equation (23) $\mathbf{E} \to -\mathbf{E}$, $d_m \to -d_m$.

[32] M. Bache, H. Guo, B. Zhou, and X. Zheng, "The anisotropic Kerr nonlinear refractive index of $\beta-BaB_2O_4$," arXiv: 1209.3158v1 (2012).

[33] F. Baronio, M. Conforti, A. Degasperis, and S. Wabnitz, " Three-wave trapponic solitons for tunable high-repetition rate pulse train generation," IEEE J. Quant. Electron. **44**, 542 (2008).

[34] F. Baronio, M. Conforti, C. De Angelis, A. Degasperis, M. Andreana, V. Couderc and A. Barthelemy, "Velocity-locked solitary waves in quadratic media," Phys. Rev. Lett. **104**, 113902 (2010).

[35] M. Bache, O. Bang, W. Krolikowski, J. Moses, and F. Wise, "Limits to compression with cascaded quadratic soliton compressors," Opt. Expr. **16**, 3273-3287 (2008).

[36] M. Bache, O. Bang, B. Zhou, J. Moses, and F. Wise, "Optical Cherenkov radiation in ultrafast cascaded second-harmonic generation," Phys. Rev. A **82**, 063806 (2010).

[37] M. Bache, O. Bang, B. Zhou, J. Moses, and F. Wise, "Optical Cherenkov radiation by cascaded nonlinear interaction: an efficient source of few-cycle energetic near- to mid-IR pulses," Opt. Expr. **19**, 22557-22562 (2010).

[38] P. Wai, C. Menyuk, Y. Lee, and H. Chen, "Soliton at the zero-group-dispersion wavelength of a single-model fiber," Opt. Lett. **12**, 628-630 (1987).